MODERN ASTRONOMY:
FROM THE EARLY UNIVERSE TO EXOPLANETS AND BLACK HOLES

Investigation of the infrared profiles of exoplanet HD 209458 b secondary eclipses

A. Fedotov[1] and R. Baluev[1,2]

[1] Saint Petersburg State University, 7–9 Universitetskaya Emb., St. Petersburg, 199034 Russia
[2] Special Astrophysical Observatory of the Russian Academy of Sciences, Nizhny Arkhyz, 369167 Russia

Abstract. In this work we process infrared light curves for 13 secondary eclipses of the exoplanet HD 209458 b, obtained with the Spitzer Space Telescope. The objective of the study was to identify any discrepancies that might be attributed to the inhomogeneity of the planet's surface brightness or a difference of the planet's shape from a sphere. Firstly, an attempt was made to ascertain whether the observed midpoint of the secondary eclipse exhibited a shift from the ephemeris moment. This could indicate the presence of a hot spot on the planet's surface that is shifted from the central meridian. The analysis allowed for the correlated noise that remained in the IRAC detector data after aperture photometry by approximating the noise with a Gaussian random process. As a result, we detected two components of red noise with different time scales: ~ 10 s and ~ 5 min. In addition, we constructed a unified model of the effect of inhomogeneous pixel sensitivity as a periodic function of the brightness centroid coordinates, which works well for all the analyzed eclipses. According to the results, the main parameters of the HD 209458 b eclipse coincided with those obtained by other authors: a depth of $0.125 \pm 0.004\%$ and a shift of the observed midpoint of -0.53 ± 0.61 min.

Keywords: planets and satellites: surfaces, general; stars: planetary systems; techniques: photometric; methods: data analysis; stars: individual: HD 209458

DOI: 10.26119/VAK2024.130

1 Introduction

The investigation of exoplanets is an important topic in modern astronomy. In the past 30 years, more than 5500 exoplanets have been discovered. It has become possible today not only to improve the methods of discovery but also to investigate planets' physical characteristics. The most significant sources of information on exoplanets are the observations of transits and secondary eclipses (events when a planet passes behind the parent star). To observe these events, it is necessary that the plane of a planet's orbit be nearly perpendicular to the picture plane. While this limits the number of planetary systems available for study, the potential for obtaining data on these systems makes them a primary target for observing efforts.

In our research, the main focus is on the study of secondary eclipses. These observations allow us to determine the orbital elements of an exoplanet and obtain information about its surface temperature. However, the main issue of our work has been the identification of a more subtle phenomenon: the uneven distribution of brightness on the planet's surface, which should affect the initial and final stages of the eclipse. Hot Jupiters are the most promising candidates for this study as they have a higher brightness relative to their parent stars and are expected to exhibit variation in the surface brightness (Rauscher & Menou 2013). The most noticeable inhomogeneities are in the infrared range, where these planets exhibit their maximum brightness.

In this study, we use the IRAC instrument data from the Spitzer Space Telescope in the 3.6 μm band. Our research focuses on the exoplanet HD 209458 b, selected due to its nearly circular orbit and large number of observations. Papers on a related topic have been published previously (Knutson et al. 2007; Majeau et al. 2012; de Wit et al. 2012). The novel aspects of this research lies in our investigation of HD 209458 b using the Gaussian random process (GP) method.

2 Data reduction

We analyzed 13 secondary eclipses. The basic calibrated data (BCD) FITS files are publicly available.[1] The observations were made between 2011 and 2015. For each eclipse we used the data within 4 hours before and after the center of the eclipse. Each eclipse consisted of 2500–3500 three-dimensional files with a size of 32×32 pixels and 64 frames in the third dimension.

We performed aperture photometry on each frame using the astropy (Astropy Collaboration et al. 2013) and photutils (Bradley et al. 2024) packages. The center

[1] https://sha.ipac.caltech.edu/applications/Spitzer/SHA/

of the aperture was determined by calculating the weighted average of the flux within a 8×8 pixel square centered on the frame. The aperture radius within which the flux was measured was 4 pixels. We subtracted the median background outside a ring with a radius of 12 pixels from the resulting flux. We removed 247 frames using the method described in Baluev et al. (2015). The outliers were detected by comparing the empirical distribution of residuals to a Gaussian. The photometric dimensions that fell into the strongly deviating tails of the distribution were removed. Finally, we binned 64 frames together. This was done to reduce the quantity of data for the next step in our work because of the limitations on available computing resources.

3 Model

We obtain a light curve that contains correlated noise. Taking this into account was the main difficulty in our work. To allow for this, we used a method that assumes that the correlated noise is a stationary Gaussian random process (the GP method). This is a development of the maximum likelihood estimation method similar to those used in Fedotov & Baluev (2022) with the use of an additional regression at the coordinates of the brightness center. The function for minimization was

$$\begin{aligned} &f(\theta,\eta) = \ln\det \mathsf{V}(\eta) + \frac{1}{\gamma}\, r^{\mathrm{T}}(\theta)\, \mathsf{V}(\eta)^{-1}\, r(\theta) \quad \overset{\theta,\eta}{\longmapsto} \quad \min, \\ &r = x - \mu(t,y,\theta), \qquad \gamma = 1 - \frac{\dim\theta}{\dim x}, \end{aligned} \tag{1}$$

where we have:

(1) input data that include the observation moments t, the primary input data x, and the auxiliary data y used in a regression model;
(2) the model μ of the curve being fitted (including possible regression against y) and the model V of the noise covariance matrix;
(3) fittable parameters θ and η.

The implementation of this method is based on the `PlanetPack` project (Baluev 2013, 2018), which is written in `C++`.

We employed two methods to analyze the data. The first approach involved correlated noise that was dependent only on time. To this end, we utilized the following

kernel function:

$$
\begin{aligned}
&k = k_{\mathrm{WN}} + k_{\mathrm{RN}} + k_{\mathrm{QPN}},\\
&k_{\mathrm{WN}}(\Delta t, \eta_{\mathrm{WN}}) = \sigma^2_{\mathrm{WN}} \times \begin{cases} 1, & \Delta t = 0,\\ 0, & \Delta t \neq 0, \end{cases} && \eta_{\mathrm{WN}} = \{\sigma_{\mathrm{WN}}\},\\
&k_{\mathrm{RN}}(\Delta t, \eta_{\mathrm{RN}}) = \sigma^2_{\mathrm{RN}} \exp\left(-\frac{\Delta t^2}{2\tau^2_{\mathrm{RN}}}\right), && \eta_{\mathrm{RN}} = \{\sigma_{\mathrm{RN}}, \tau_{\mathrm{RN}}\},\\
&k_{\mathrm{QPN}}(\Delta t, \eta_{\mathrm{QPN}}) = \sigma^2_{\mathrm{QPN}} \exp\left(-\frac{\Delta t^2}{2\tau^2_{\mathrm{QPN}}}\right) \cos\frac{2\pi\Delta t}{P_{\mathrm{QPN}}}, && \eta_{\mathrm{QPN}} = \{\sigma_{\mathrm{QPN}}, \tau_{\mathrm{QPN}}, P_{\mathrm{QPN}}\}.
\end{aligned}
\tag{2}
$$

It consists of three main components: white noise, red noise, and quasi-periodic noise. However, an analysis of the intermediate data indicates that the model does not accurately match the autocorrelation function. In order to improve the approximation, a second component of red noise was added. This resulted in the final kernel function being

$$k = k_{\mathrm{WN}} + k_{\mathrm{RN1}} + k_{\mathrm{RN2}} + k_{\mathrm{QPN}}. \tag{3}$$

In the second approach we considered the dependence of the noise component not only on time but also on the coordinates of the brightness centroid. Initially, we used a single model for the pixel sensitivity map for each eclipse, which was responsible for the received flux. The model was a two-dimensional Fourier series:

$$
\begin{aligned}
\mu(x,y) = {} & a_1\cos(2\pi x) + b_1\sin(2\pi x) + a_2\cos(2\pi y) + b_2\sin(2\pi y)\\
& + a_3\cos(2\pi(x+y)) + b_3\sin(2\pi(x+y))\\
& + a_4\cos(2\pi(x-y)) + b_4\sin(2\pi(x-y)) + c.
\end{aligned}
\tag{4}
$$

Nevertheless, the realization of the model demonstrated a tendency to degeneration. This was caused by small shifts (approximately 0.04 pixels) of the brightness centroid coordinates during observation of one eclipse. As a consequence, some components in the model became correlated. In order to overcome this issue, each eclipse was considered separately, with the basis functions decomposed in Taylor series around zero and the dependent elements eliminated. The outcome of this process was the creation of a new model, which was subsequently employed in our research:

$$
\begin{aligned}
\mu(x,y) = {} & a_1\sin(2\pi\Delta x) + a_2 2\sin^2(\pi\Delta x) + b_1\sin(2\pi\Delta y) + b_2 2\sin^2(\pi\Delta y)\\
& + d_2\sin(2\pi\Delta x)\sin(2\pi\Delta y) + c.
\end{aligned}
\tag{5}
$$

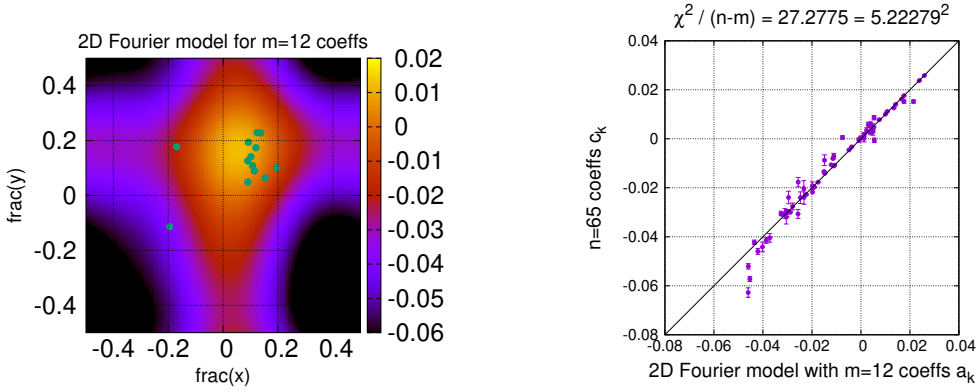

Fig. 1. Left: systematic error in fractions of the total flux as a function of the coordinates of the brightness center. Right: ratio between the 2D Fourier model and GP model coefficients.

It is also important to note that the use of approximation did not entirely remove the noise component from the data. Consequently, the model retained both red and white noise, and the kernel function became:

$$k = k_{\mathrm{WN}} + k_{\mathrm{RN}}. \tag{6}$$

Furthermore, it is necessary to consider the model of the eclipse constructed in conjunction with the noise. The planet in the model is spherical in shape and has a uniformly bright disk, which corresponds to the most basic model presented in Baluev & Shaidulin (2015). During the eclipse, the model planet moves uniformly and linearly with a certain impact parameter. In this study we did not utilize the transit data, which would have enabled us to accurately restore the characteristics of the planet. Instead, we relied on the parameters from another work (Bonomo et al. 2017) to determine the characteristics. We approximated two parameters only: the ratio of the planet's brightness to that of the star and the shift of the center of the eclipse compared to a model with zero eccentricity.

In order to account for long-period red noise, a third-order polynomial was employed. The noise parameters were considered individually for each eclipse, while the eclipse parameters were shared among all 13 eclipses.

4 Result

As a result, the next values were obtained: an eclipse center shift of 0.93 ± 3.10 min and a brightness ratio of $0.102 \pm 0.014\%$ for the first approach and -0.53 ± 0.61 min and $0.125 \pm 0.004\%$ for the second approach. These data are in agreement with the

results obtained by other authors (Evans et al. 2015). An important result is also the detection of two components of red noise in the first approach on time scales of 10 s and 5 min. In Evans et al. (2015) the red noise for different eclipses takes alternating values from one or the other of these scales. Also, the second approach allowed us to construct an overall pixel sensitivity map (Fig. 1). Although no noticeable deviations of the eclipse profile from the uniformly bright disc model could be detected (Fig. 2), the developed technique lays the foundation for more extensive work on processing the observed data from other planetary systems.

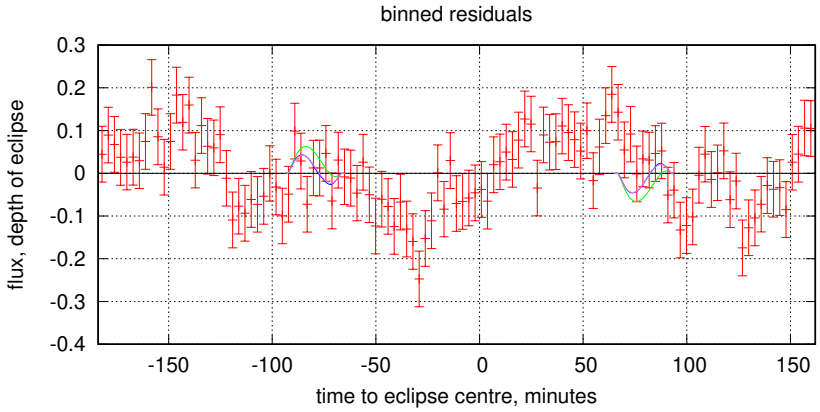

Fig. 2. Model residuals binned in 3-min intervals and the deviations due to brightness inhomogeneities from Rauscher & Menou (2013): black—uniform brightness, green—model 0 G, blue—model 3 G, violet—model 10 G.

References

Astropy Collaboration, Robitaille T.P., Tollerud E.J., et al., 2013, A&A, 558, id. A33
Baluev R.V., 2013, Astronomy and Computing, 2, p. 18
Baluev R.V., 2018, Astronomy and Computing, 25, p. 221
Baluev R.V. and Shaidulin V.S., 2015, MNRAS, 454, 4379
Baluev R.V., Sokov E.N., Shaidulin V.S., et al., 2015, MNRAS, 450, p. 3101
Bonomo A.S., Desidera S., Benatti S., et al., 2017, A&A, 602, id. A107
Bradley L., Sipőcz B., Robitaille T., et al., 2024, astropy/photutils: 1.13.0
de Wit J., Gillon M., Demory B.O., et al., 2012, A&A, 548, id. A128
Evans T.M., Aigrain S., Gibson N., et al., 2015, MNRAS, 451, p. 680
Fedotov A.A. and Baluev R.V., 2022, Astronomy at the Epoch of Multimessenger Studies, Proc. All-Russian Astron. Conf. (VAK-2021), p. 227
Knutson H.A., Charbonneau D., Allen L.E., et al., 2007, Nature, 447, p. 183
Majeau C., Agol E., Cowan N.B., 2012, ApJL, 757, id. L32
Rauscher E. and Menou K., 2013, ApJ, 764, p. 103